IEEE Access
Multidisciplinary | Rapid Review | Open Access Journal

Received June 14, 2019, accepted July 12, 2019, date of publication July 16, 2019, date of current version August 13, 2019.

Digital Object Identifier 10.1109/ACCESS.2019.2929261

Application of Superconductors to Improve the Performance of DFIG-Based WECS

MOHAMMED I. MOSAAD[1], AHMED ABU-SIADA[2], AND MOHAMED F. EL-NAGGAR[3,4]

[1]Yanbu Industrial College, Yanbu 46452, Saudi Arabia
[2]Electrical and Computer Engineering Department, Curtin University, Bentley, WA 6152, Australia
[3]Electrical Engineering Department, College of Engineering, Prince Sattam Bin Abdulaziz University, Al-Kharj 11942, Saudi Arabia
[4]Department of Electrical Engineering, Helwan University, Cairo 11795, Egypt

Corresponding author: Mohammed I. Mosaad (m_i_mosaad@hotmail.com)

This work was supported in part by the Deanship of Scientific Research, Prince Sattam Bin Abdulaziz University, under Project 2017/ 01/ 7126.

ABSTRACT This paper presents a new cost-effective technique to improve the performance of doubly fed induction generator (DFIG)-based wind energy conversion systems (WECS) during wind gust and fault events through the integration of high temperature superconductor (SC) within the DC link of the rotor side and grid side converters that interface the DFIG rotor with the grid. Fractional order proportional integral (FOPI) controller is employed to control the energy exchange between the SC and the system through controlling the duty cycle of the DC chopper interfacing the SC with the DC link. Rating of the SC and parameters of the proposed FOPI controller are precisely calculated using harmony search optimization technique in order to regulate the DFIG generated power and improve its fault ride through capability during disturbance events. To validate the superiority of the proposed FOPI controller, the performance of the studied system is also investigated when a conventional PI controller is employed. Results reveal the ability of the proposed topology and controller to improve the performance of the DFIG-based WECS during wind gust and short circuit faults at the DFIG terminals.

INDEX TERMS Superconductors, doubly fed induction generator, wind energy conversion system, harmony search optimization, fractional order PI.

I. INTRODUCTION

Doubly fed induction generators (DFIGs) are currently dominating the market of wind energy conversion systems (WECS) due to the low rating of the converters interfacing the DFIG rotor with the grid, wide speed operational range and capability of controlling active and reactive powers [1]–[3]. The DFIG-based WECS also features more power capture, better power quality, reduced mechanical stress on the drivetrain when compared with fixed speed wind turbines [4]. On the other hand, the main drawback of the DFIG is its sensitivity to grid disturbances, weak fault ride through (FRT) capability and the fluctuation in the generated power [5]–[7]. Fluctuation in the DFIG output power may occur during normal operation due to wind gust [8]. If not properly regulated, power fluctuation may result in adverse effects on power system stability, quality, voltage and frequency. During the first generation, a wind turbine was allowed to be disconnected from the grid during various fault events to avoid potential damages to the electronic and mechanical systems [9], [10]. With the growth in WECS installations, which contribute a significant portion of the power demand, the transmission line operators have set strict grid codes to maintain wind turbine operation to support the grid during various fault events [11]. As such, much attention was given to improve the FRT capability of the DFIG. A crowbar protection circuit connected across the rotor side converter (RSC) was proposed to bypass the large current generated during short circuit faults [12]. Consequently, the DFIG is converted into a squirrel cage induction generator that absorbs reactive power from the grid [13].

To alleviate the voltage profile at the point of common coupling (PCC) during fault events, shunt flexible AC transmission system (FACTS) such as static var compensator [14], [15] and static synchronous compensator [16] with proper controller are proposed in the literatures. Series compensator such as dynamic voltage restorer is also proposed [17]. Superconducting magnetic energy

The associate editor coordinating the review of this manuscript and approving it for publication was Yunfeng Wen.

This work is licensed under a Creative Commons Attribution 4.0 License. For more information, see http://creativecommons.org/licenses/by/4.0/

storage (SMES) is proposed to improve the FRT of a hybrid power system comprising photovoltaic and DFIG-based WECS [18].

The above-mentioned techniques call for the connection of extra device that is interfaced with the grid through additional power converters which complicates the implementation and increases the cost of these techniques.

To overcome these issues, a new topology for the back-to-back converters that interface the DFIG rotor with the grid through integrating a high temperature superconductor (SC) was proposed in [19] in which the SC is connected to the DC link through a DC-DC chopper. However, the rating of the proposed SC was not precisely calculated. Moreover, the proposed fuzzy logic-based controller is complicated and does not achieve satisfactory performance during various disturbance events. A SC-based fault current limiter to enhance the DFIG low voltage ride through capability and to regulate the generated power was proposed in [20]. However, the proposed control strategy calls for the change in the control system of DFIG conventional converters which makes the proposed technique only suitable for new DFIG-WECS installation. Furthermore, no specific optimum calculation for the SC rating was provided.

The main drawback of SC lies in its cost and sensitivity to the controller used to drive it. Hence, proper optimization to reduce the SC size without compromising its performance is essential. No much attention was given in the literatures to properly optimize the SC size along with the control system parameters. A multi-objective function for optimum design of a SC integrated into DFIG-WECS using particle swarm optimization (PSO) is presented in [21], [22]. The parameters of the proportional integral (PI) controller used to control the duty cycle of the DC-DC chopper were also tuned using PSO. However, the performance of PSO and PI controller is not satisfactory when compared with the recent modern optimization techniques and the fractional order proportional integral (FOPI) controller, respectively. In [23], a new optimization technique namely harmony search (HS) is employed to identify optimum tuning of the PI control parameters to improve the power quality of a grid-connected fuel cell. Results in [23] reveal that HS optimization technique provides better performance than PSO. On the other hand, and as reported in [24], [25], the FOPI controller provides better performance than the conventional PI controller. FOPI was also reported to provide a better performance than conventional PI in controlling a voltage source converter used in microgrid applications [26].

From the above discussion, the new contribution of this paper can be summarized as below:

- proposing a new topology of a SC within the DC link of the DFIG converters without changing existing WECS infrastructure.
- developing a simple and reliable FOPI controller to regulate the energy exchange between the SC and the DC link during disturbance events.
- optimizing the SC size to reduce the implementation cost without compromising its performance.
- optimizing the FOPI controller parameters in order to attain reliable control performance.

II. SYSTEM DESCRIPTION

The studied system consists of six wind turbines of 1.5 MW each, 575V, 60 Hz DFIGs connected to the network at a point of common coupling (PCC) as shown in Fig.1. The grid is simulated as an infinite bus of constant voltage and frequency (120 kV, 60 Hz). A short transmission line (TL) of 30 km connects the grid and the DFIG stator via a step-up coupling transformer while the rotor and the coupling transformer are interfaced through rotor side converter (RSC) and grid side converter (GSC). The proposed SC is connected to the DC link of the two converters through DC-DC chopper of which the duty cycle is controlled to regulate the energy exchange between the SC and the system during disturbance events. The SC ratings are 3.5KA, 0.25 H and 900V.

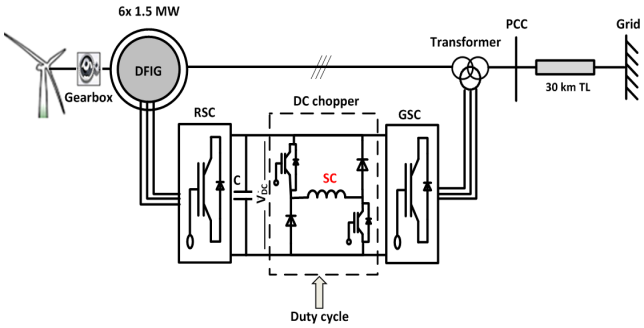

FIGURE 1. DFIG-based WECS under study with the inclusion of SC.

The SC is initially charged to its maximum capacity by maintaining the voltage across its terminals at the maximum rated level. When the current and hence the stored energy reach maximum levels, the stored energy is retained by short-circuiting the SC using a flywheel diode. The control of the chopper duty cycle should act to exchange energy between the coil and the system during disturbance events only. During normal operation there should be no energy transfer between the SC and the system. During normal operation, the conventional control system of the GSC and RSC is applied. DFIG detailed dynamic modeling can be found in [27]. A brief description of the conventional GSC and RSC vector control systems are presented below.

A. GSC CONVENTIONAL CONTROL SYSTEM

GSC controls the energy exchange between the grid and the DC-link capacitor and retains the capacitor voltage within acceptable levels [28]–[30]. This task is performed by taking the voltage across the DC-link as a feedback signal that is compared with a predefined voltage reference to generate the d-axis component of the stator current i_{dg}^{*} that is compared with actual d-axis stator current i_{dg} which is generated by

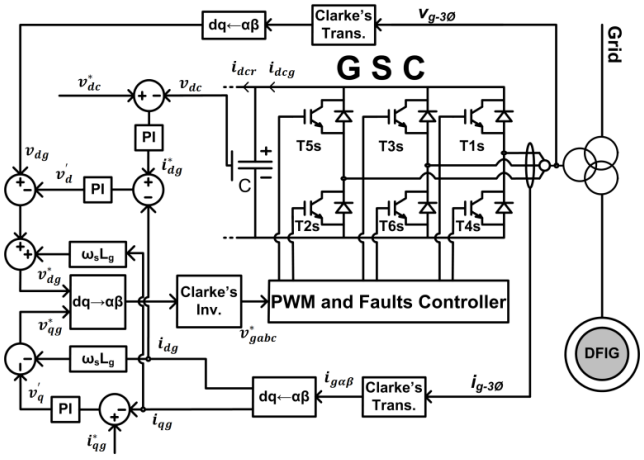

FIGURE 2. GSC conventional control system.

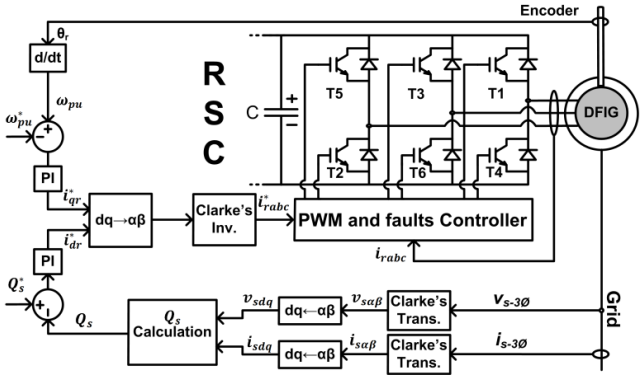

FIGURE 3. RSC conventional control system.

converting the actual stator terminal currents into d-q reference frame as shown in Fig.2 [30].

The d-axis stator current error signal is fed into a PI controller. Similarly, the q-axis stator current error is fed to another PI controller. The output of the two PIs are used to generate d-q reference voltage signals that are controlling the pulse width modulation (PWM) circuit to generate proper firing pulses for the GSC switches.

B. RSC CONVENTIONAL CONTROL SYSTEM

RSC controls the DFIG generated active power based on rotor speed while the terminal voltage is regulated through DFIG reactive power support [28]–[30]. Maximum power is tracked by selecting a proper speed reference signal ω^*_{pu} based on the wind turbine characteristics. This reference signal is compared with the actual rotor speed. The speed error signal is fed into a PI controller to generate q-axis rotor current i^*_{qr}. To realize unity power factor at the DFIG terminals, the reactive power reference Q^*_S is set to zero and is compared with the calculated reactive power using the stator terminal voltage and current as shown in Fig. 3 [30].

The reference rotor d-axis current i^*_{dr} is generated through feeding the reactive power error signal to another PI controller. Clarke-Park transformation is used to convert the d-q current components to a-b-c reference frame that is controlling the PWM circuit to generate proper firing pulses for the RSC switches.

III. PROPOSED SUPERCONDUCTOR CONTROL SYSTEM

The main objective of the SC proposed control system is to enhance the FRT capability of the DFIG during short circuit faults at the PCC and to regulate the DFIG output power fluctuation due to wind gust. The HS optimization technique is employed to calculate the optimum rating of the SC and the parameters of the FOPI controller.

The FOPI controller has gained significant attention during the last decade in the science and engineering applications [24], [25], [31]. This controller is characterized by a fractional integral involving an integrator of order λ, where $\lambda \in R$. The transfer function $G(s)$ of the FOPI controller is given by:

$$G(s) = k_p + \frac{k_i}{s^\lambda} \tag{1}$$

where k_p and k_i are respectively the FOPI proportional and integral constants and λ is the fractional integration order. In case of conventional PI controller, $\lambda = 1$.

The duty cycle (D) of the chopper determines the mode of operation of the SC through the polarity of the voltage across the coil (V_c) based on the equation below.

$$V_c = (1 - 2D)V_{DC-link} \tag{2}$$

where $V_{DC-link}$ is the voltage across the DC link capacitor.

Based on the value of D, there are three operational modes for the SC. Idle mode is when $D = 0.5$ at which the voltage across the SC is maintained at zero level and no energy exchange takes place between the SC and the system. Discharging mode is when $D > 0.5$ at which the SC exhibits negative voltage across its terminals and energy stored in the coil is discharged to regulate the active and reactive power at the PCC during disturbance events. Where there is any surplus power in the system the SC charging mode is activated with a chopper duty cycle value lies in the range $0 < D < 0.5$. the magnitude of D controls the amount of energy exchange between the coil and the DC link. It is to be noted that the current through the SC is always unidirectional and energy exchange is achieved through the change of the slope of the SC current (di/dt). The control system proposed in this paper is triggered by the voltage level at the PCC (V_{PCC}) that identifies two control modes. If $|V_{PCC}| \geq 0.9$ pu, mode 1 for the power fluctuation control is activated. On the other hand, if $|V_{PCC}| < 0.9$ pu, mode 2 for FRT enhancement is triggered. The two control modes are shown in Fig. 4 and are explained below.

A. MODE 1, POWER FLUCTUATION CONTROL

This control mode is aimed at smoothing the DFIG output power fluctuation due to wind gust while the voltage

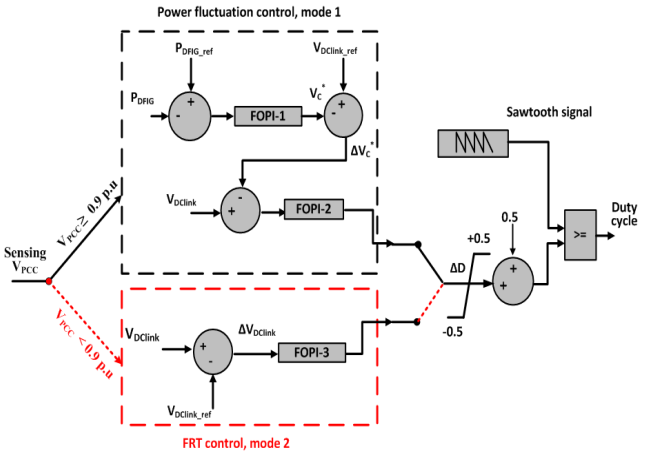

FIGURE 4. Proposed SC two control modes using FOPI.

profile at the PCC is within the IEEE standard limits of ±10% [32], [33]. As shown in Fig. 4, this mode employs two FOPI controllers; FOPI-1 and FOPI-2 that comprise 6 parameters (K_{p1}, K_{i1}, λ_1, K_{p2}, K_{i2} and λ_2).

The difference of the DFIG output power (P_{DFIG}) and a predefined reference power (P_{DFIG_ref}) is used as an input to the FOPI-1 whose output is an updated voltage value (V_C^*) that is correlated to the DFIG output power change due to wind speed variation. The value of V_C^* is compared with the reference value of the DC link voltage to generate an error signal ΔV_C*. This signal is then compared to the measured voltage across the DC link and the difference is fed to FOPI-2 to generate a proper duty cycle deviation (ΔD). The duty cycle deviation is normalized to a value between 0 and 1 that is used with a sawtooth signal to create the final DC chopper duty cycle value.

B. MODE 2, FRT CONTROL

Without SC and during faulty conditions at the PCC, the GSC cannot exchange power with the network and the voltage across the DC link will exhibit significant oscillations. With optimally controlled SC, the energy stored in the coil can be rapidly released to improve the DC-link voltage profile during fault events. The third controller, FOPI-3, is aimed at enhancing the FRT capability of the DFIG during faults at the PCC by maintaining the DC-link voltage at nearly constant value. This controller is activated when the PCC voltage profile becomes less than 0.9 p.u. In this control mode, the DC link voltage at the PCC is sensed and compared with the reference DC voltage as shown in Fig. 4. The error signal is fed to the third controller FOPI-3 which comprises three parameters (K_{p3}, K_{i13} and λ_{13}). The output of this controller is the duty cycle deviation that is normalized in a range of 0 to 1 as stated above.

A comparison of the performance of conventional PI and the proposed FOPI controllers for the above two control modes is investigated by replacing the three FOPI controllers in Fig. 4 by three conventional PI controllers that comprise six parameters K_{p1_pi}, K_{i1_pi}, K_{p2_pi}, K_{i2_pi}, K_{p3_pi} and K_{i3_pi}.

IV. HARMONY SEARCH OPTIMIZATION

HS is one of the recently developed optimization techniques that has been proposed in several power and renewable energy systems studies [23], [32]–[34]. HS optimization technique demonstrated higher efficiency and performance than performance than PSO and GA as introduced in [23]. In this paper, HS is used to optimize the SC size and to tune the FOPI/PI control parameters. Thus, the main objective of the HS is to determine the minimum SC size with minimum initial energy stored. Also, HS is manipulated to identify the optimum parameters of the three FOPI/PI controllers to achieve satisfactory performance of the DFIG-based WECS during wind gust and disturbance events. Each FOPI/PI controller has three/two parameters, so nine/six parameters are required to be optimized for the two controllers.

An objective function J is constructed for the optimum SC size (inductance, L_{sc}), optimum initial current in the SC (I_{sco}) and optimum FOPI/PI control parameters for power fluctuation and FRT of the studied system. Hence, the objective function comprises four terms as below.

$$J = W_1.E_0 + W_2 \int |\Delta V_{dc}|\, dt + W_3 \int |\Delta P|\, dt + W_4 \int |\Delta I_R|\, dt \quad (3)$$

with the following constrains:

$$0.001H \le L_{sc} \le 10\,H,$$
$$1kA \le I_{sco} \le 5\,kA,$$

and all control parameters are of positive values.

In (3), ΔV_{dc} is the difference between the actual and reference DC-link voltage, ΔP is the difference between the actual and reference DFIG power, ΔI_R is the difference between the actual and reference GSC current, I_{sco} is the initial SC current, $E_0 = 0.5 L_{sc} I_{sco}^2$ is the SC initial energy stored and W_1 to W_4 are arbitrary weighting factors in the range 0 to 1.

Any change in the wind speed and faults at the PCC will cause deviations in the DFIG output power ΔP and the DC link voltage ΔV_{dc}. These deviations are to be minimized through the proposed objective function J.

The values of the weighting factors W_1 to W_4 are set as 1, 0.5, 0.2 and 0.3 respectively [22]. The first term in the objective function is related to the SC optimum design and includes the initial energy stored ($E_0 = 0.5 L_{sc} I_{sco}^2$) in the coil. Thus a full weighting factor of 1 is selected for this term in the objective function. The second term is related to the FRT (control mode-2) that is used to determine the optimum control parameters of the FOPI-3 controller. The weighting factor of this term (W_2) is set to 0.5 as only one FOPI control parameters are calculated using this term in the objective function. The third and fourth terms are related to the power fluctuation smoothing control mode (control mode-1). These two terms are used to calculate the parameters of the FOPI-1

and FOPI-2 controllers. Therefore, W_3 and W_4 must add up to a value of 0.5; in the proposed objective function, W_3 is set to a value of 0.2 while W_4 is set to a value of 0.3. The objective function J is used to optimize eleven parameters, two for the SC design and nine for the three FOPI controllers. For the PI controllers, the same objective function is attained by replacing the three FOPI controllers by three conventional PI controllers.

The first step in HS is the initialization of the eleven parameters by assuming random values within their acceptable ranges. Based on these random values, the fitness function J is calculated according to (3). Then the Harmony Memory (HM) is formed as in the matrix below [34]–[36].

$$HM = \begin{bmatrix} L_{sc}^1 & I_{sco}^1 & K_{p1}^1 & K_{i1}^1 & \lambda_1^1 & \cdots & \lambda_3^1 \\ L_{sc}^2 & I_{sco}^2 & K_{p3}^2 & [K_{i3}^2] & \lambda_3^2 & \cdots & \lambda_3^2 \\ \vdots & \vdots & \vdots & \vdots & \vdots & \vdots\ \vdots & \vdots \\ L_{sc}^{HMS} & I_{sco}^{HMS} & K_{p1}^{HMS} & K_{i1}^{HMS} & \lambda_1^{HMS} & \cdots & \lambda_3^{HMS} \end{bmatrix} \quad (4)$$

The HM matrix comprises 11 columns for the FOPI controller parameters and 8 columns when PI controllers are utilized. Each row in the HM matrix represents an improved harmony vector based on the harmony memory considering rate (HMCR) and pitch adjusting rate (PAR). The updated harmony vector x_i^{n+1} of the current harmony vector x_i^n is conducted as below:

$$x_i^{n+1} = x_i^n + rand * BW \quad (5)$$

where *rand* is a random value between (0,1) and BW is an arbitrary distance bandwidth.

The updating process is repeated until a minimum possible value for the objective function J or a maximum search number has been reached as per the flow chart of Fig. 5.

V. RESULTS AND DISCUSSIONS

The HS optimization technique is used to determine the minimum SC coil size and the optimum parameters for the proposed FOPI and PI controllers in order to improve the performance of the investigated DFIG-based WECS (shown in Fig. 1) during fault and wind gust events. The fluctuation in the DFIG generated power is simulated through a rapid change in the wind speed between 10.5 m/s and 19.5 m/s within a short duration (5 s) as shown in Fig. 6. On the other hand, the DFIG FRT capability is assessed when an intermittent three-phase short circuit fault is assumed to take place at the PCC within the period 2s to 2.25s.

The optimized parameters obtained using the HS technique are listed in Tables 1. The convergence profile of the objective function J using HS is depicted in Fig.7 which shows the best fitness of J when employing FOPI and PI controllers. Fig. 7 reveals that tuned parameters of a conventional PI controller converge at iteration number 30 while FOIP parameters converge at iteration number 32. This is attributed to the additional FOPI fractional integration parameter. The convergence of each term in the objective function for PI and FOPI controllers are also shown in Fig. 7. Results in Table 1 reveal that the rating of the SC coil is lower when FOPI controller is employed.

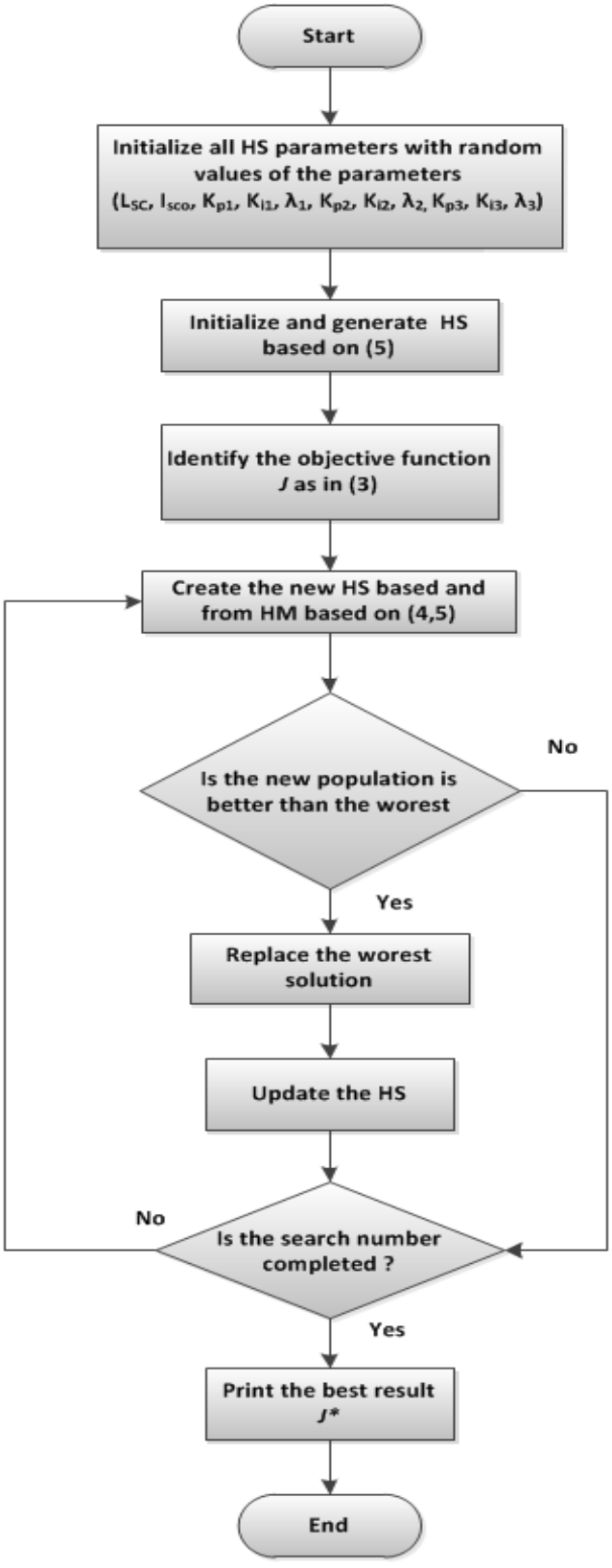

FIGURE 5. Flow chart of HS optimization for FOPI controllers.

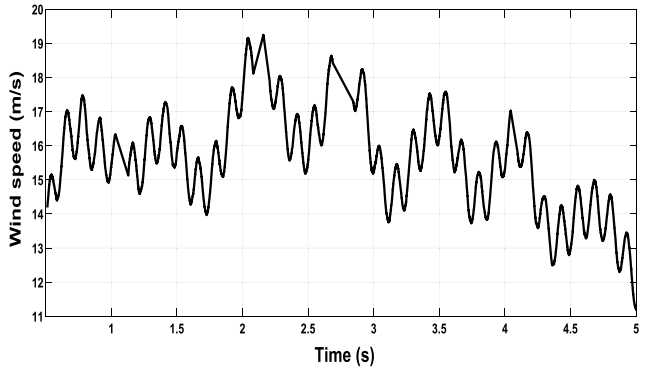

FIGURE 6. Wind gust speed pattern.

The robustness of the proposed controller is assessed through the following case studies.

A. CASE STUDY 1: DFIG POWER REGULATION

In this case study the power fluctuation control mode (mode-1) is tested for two wind speed patterns; a step change in the average wind speed and a rapid speed variation within a short period.

1) STEP CHANGE IN THE WIND SPEED

In this case study, an average wind speed is assumed to be constant at 15m/s and exhibits a step change to 17m/s within the period 3s to 5s after which the initial average wind speed level is retained. The effect of such wind speed change has insignificant impact on the voltage at the PCC as shown in Fig. 8(a) as the voltage level remains within the permissible threshold limits of ±10%. Hence according to the proposed controller in Fig. 4, the power control mode is activated.

While the voltage profile at the PCC is within acceptable limits, zooming on Fig. 8(a) shows an improved profile when the proposed SC is employed, in particular with the FOPI controller. The step change in the wind speed results in a ramp increase in the DFIG output active power that decreases when the wind speed falls down at 5s as shown in Fig. 8(b). When the proposed power control mode is activated, the fluctuation in the DFIG power is significantly suppressed when a PI controller is used. These fluctuations are fully suppressed and the DFIG output power is regulated at nearly 1p.u. regardless the step change in the wind speed when the proposed FOPI is employed. Fig. 8(c) reveals that the aggressive oscillations of

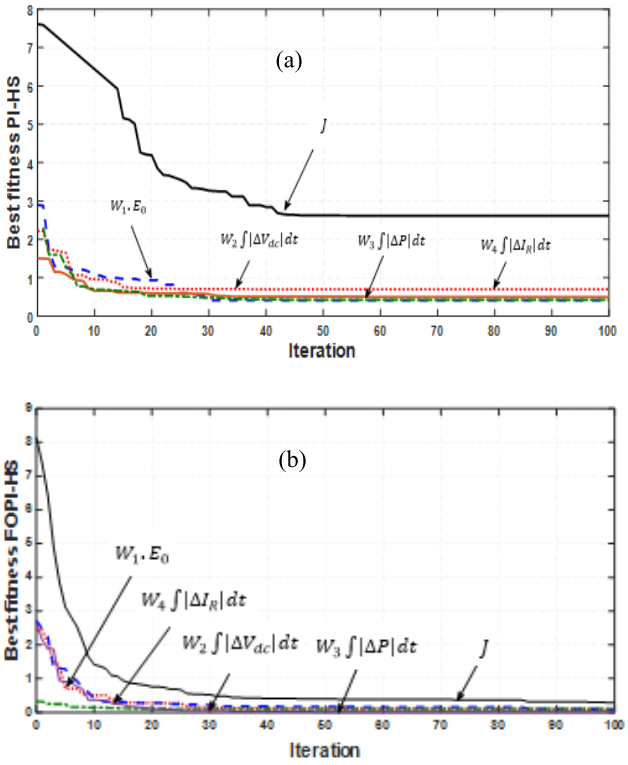

FIGURE 7. Convergence of HS optimization (a) PI controllers and (b) FOPI controllers.

the DC link voltage are damped when the power control mode is activated. The control effect is more pronounced when the FOPI is employed as it can limit the peak oscillations of the DC link voltage to a value less than ±0.2% of the nominal level.

2) RAPID WIND SPEED VARIATION

In this case study, the robustness of the power control mode is assessed during a wind gust event shown in Fig. 6. As can be seen in Fig. 9(a), due to such wind pattern, the voltage at the PCC is increasing and it comprises significant low frequency oscillations within the investigated period but it is still remaining at a level higher than 0.9 p.u. which will trigger the power control mode. By connecting the SC coil, the voltage profile is improved and the oscillations are substantially suppressed. As in the above case study, performance of the SC with the FOPI controller outperforms the conventional PI

TABLE 1. Results of the HS for optimum design of the SC and FOPI/ PI control parameters.

	SC design		FOPI / PI optimal parameters								
PI	L_{SC}(H)	I_{sco}(kA)	K_{p1_pi}	K_{i1_pi}	K_{p2_pi}	K_{i2_pi}	K_{p3_pi}	K_{i3_pi}			
	0.205	3.26	0.07	0.31	0.7	0.7	0.032	0.05			
FOPI	L_{SC}(H)	I_{sco}(kA)	K_{p1}	K_{i1}	λ_1	K_{p2}	K_{i2}	λ_2	K_{p3}	K_{i3}	λ_3
	0.19	3.1	0.3	0.5	0.79	1.6	3.4	0.85	0.6	0.95	0.76

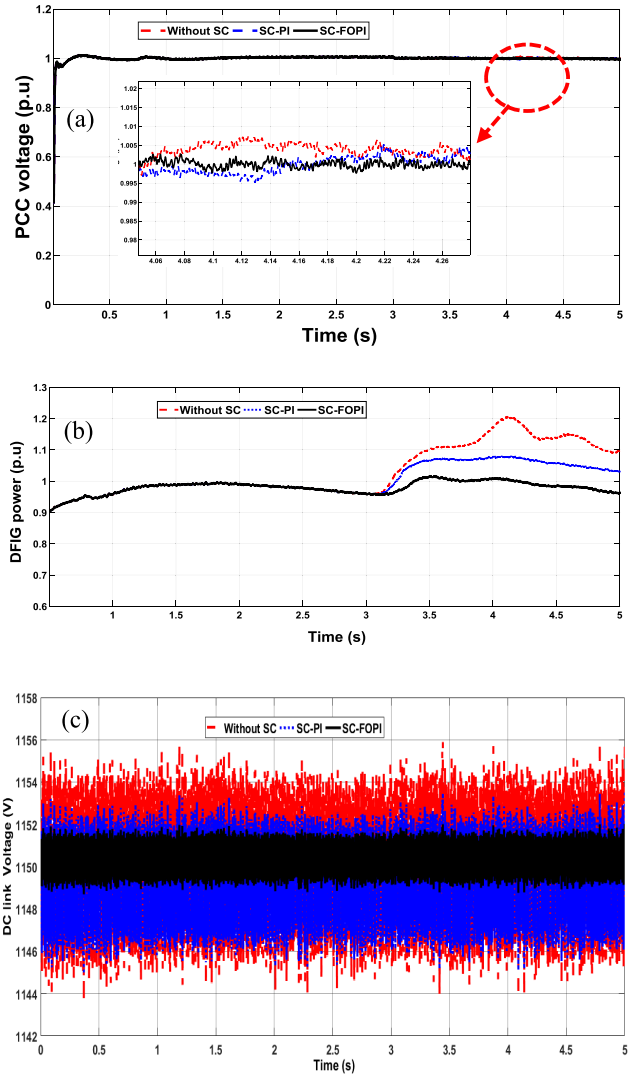

FIGURE 8. DFIG performance during a step change in the wind speed with and without the proposed controller (a) PCC voltage, (b) DFIG active power, and (c) DC link voltage.

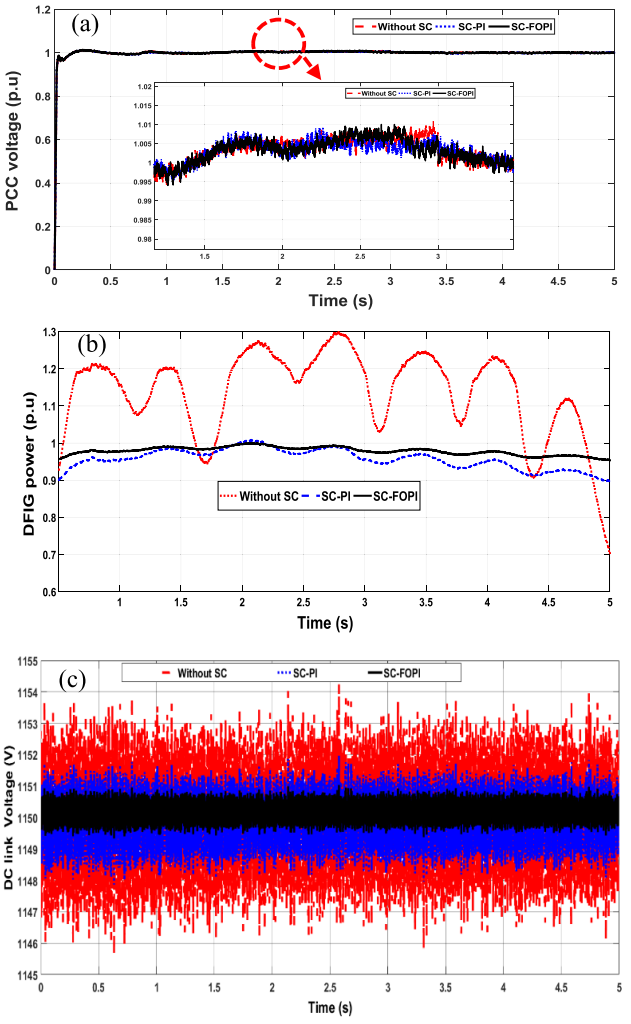

FIGURE 9. DFIG performance during a wind gust with and without the proposed controller (a) PCC voltage, (b) DFIG active power, and (c) DC link voltage.

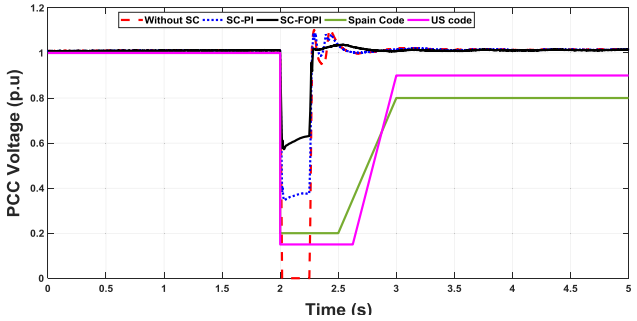

FIGURE 10. PCC voltage during a 3-phase short circuit at the PCC with and without the proposed controller.

controller performance. As can be seen in Fig. 9(b) without the connection of the SC and because of the wind gust, the DFIG power is oscillating and reaches a crest value of 1.3 p.u. The improvement in the DFIG active power is clearly observed when the SC is connected to the DC link with any of the proposed controllers especially the FOPI that can maintain the power at its nominal value. Fig. 9(c) shows that without the SC, the oscillations within the DC link voltage are significant and the voltage reaches a crest value of 1155 V. When the SC along with the PI controller is employed, an observable improvement in the voltage profile can be realized. The SC with the FOPI controller can significantly reduce the DC link peak voltage to 1150.5 V.

B. CASE STUDY 2: FAULT RIDE THROUGH

The robustness of the proposed controller to enhance the FRT capability of the DFIG-based WECS is assessed when an intermittent 3-phase short circuit fault takes place at the PCC within the period 2s to 2.25s. An average wind speed of 15m/s is assumed for this case study. As can be seen in Fig. 10, without the connection of the SC, the voltage at the PCC is reduced to zero level within the fault duration. This 100% voltage sag will violate the low voltage level of most of the grid codes and calls for the disconnection of the wind turbine to avoid any potential consequences (US and

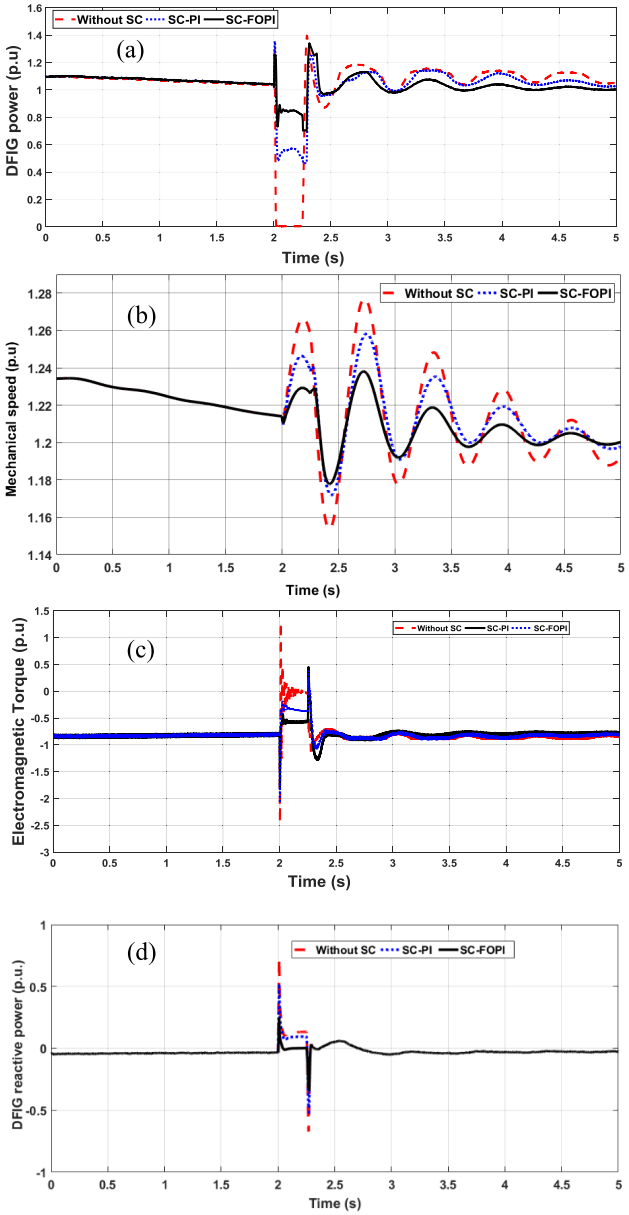

FIGURE 11. DFIG performance during a 3-phase short circuit at the PCC with and without the proposed controller (a) DFIG active power, (b) DFIG shaft speed, (c) Electromagnetic torque, and (d) DFIG reactive power.

Spain low voltage ride through (LVRT) limits are provided as an example). As shown in Fig. 10, with the SC connected to the DC link, reactive power at the PCC is modulated and the voltage profile is significantly improved and reaches a level of 0.38 p.u. in case of PI controller and 0.58 p.u. in case of FOPI controller. With both controllers, the PCC low voltage level will be raised to a safe limit with respect to the two investigated LVRT grid codes and hence the connection of the wind turbine to the grid can be maintained during such fault event.

Due to three-phase short circuit fault at the PCC, the DFIG active power experiences a significant reduction and reaches zero level at which the shaft speed accelerates to compensate this reduction as can be seen in Fig. 11(a) and (b) respectively. When the 3-phase short circuit fault is cleared at t = 2.25s, the DFIG starts to retain its normal operation. However, the power does not settle down to its original level.

With the utilization of the SC and the proposed controllers, an observable improvement can be seen in the active power and DFIG shaft speed in terms of reduced maximum overshooting and rapid settling time. Improvement is more pronounced in case of FOPI that reduces the drop in power form 100% to only 20% and restores the nominal level of power after fault clearance. With the FOPI controller, the maximum overshooting in the shaft speed is reduced to 5% and the settling time is substantially improved.

Fig. 11(c) shows that in the absence of the SC, the DFIG electromagnetic torque experiences a momentary torsional oscillation between -2.465p.u. and $+1.29$p.u. at the moment of fault occurrence. Whereas with the SC, the electromagnetic torque profile is greatly enhanced, particularly with the FOPI controller.

During normal conditions, the DFIG is operating at nearly unity power factor as can be seen from the DFIG reactive power that is close to zero level (Fig. 11(d)). When the fault occurs and the voltage at the PCC drops to zero, a reactive power is generated to compensate the voltage reduction. When the fault is cleared, normal operation will be retained. Without the connection of the SC coil, a significant amount of reactive power (± 0.6pu) will flow through the system at the instant of fault occurrence and clearance. The connection of the SC with the proposed controller significantly reduces the maximum overshooting in reactive power due to the energy discharged from the SC to support the system during fault events.

The performance of the SC during the investigated 3-phase short circuit fault using the FOPI and PI controllers is shown in Fig. 12. The current through the coil is shown in Fig. 12(a). Before the fault, the current is almost constant and is maintained at its maximum positive level. It can be observed that the coil current is less when using FOPI controller. When the current is maintained constant, the voltage across the coil is zero as shown in Fig. 12(b) and maximum energy is stored in the coil. At this mode of operation, there is no energy exchange between the coil and the system. When the fault occurs at 2 s, the coil current reduces with a negative slope (di/dt) which changes the voltage across the coil to a negative value and coil stored energy is discharged to the DC link capacitor. When the fault is cleared at t = 2.25s, the current and voltage retain their designated limits during idle mode. The performance of the coil with the FOPI controller is better than its performance with the PI controller in terms of the amount of energy that can be released to the system. The superiority of the FOPI over conventional PI controller can be validated through comparing the performance of the two controllers during the above three-phase short circuit fault case study. Table 2 shows a performance comparison of the two controllers based on the simulation results of Fig. 11. The table and Fig. 12 clearly reveal that FOPI outperforms the conventional PI controller in terms of the amount of active

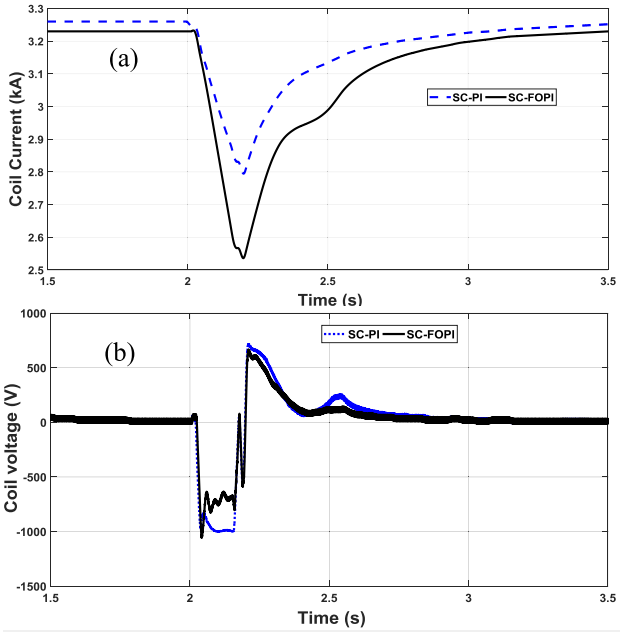

FIGURE 12. Performance of the SC coil during the 3-phase short circuit fault at the PCC.

TABLE 2. Performance of FOPI and PI during three-phase short circuit at PCC.

Min./Max value	Without SC	PI	FOPI
PCC voltage (p.u.)	0	0.35	0.58
DFIG real power (p.u.)	0	0.51	0.72
DFIG reactive power (p.u.)	0.7	0.5	0.28
Mechanical speed (p.u.)	1.275	1.25	1.23
Electromagnetic torque (p.u.)	1.2	0.4	0.38

and reactive powers that can be modulated by the SC during short circuit fault at the PCC.

VI. CONCLUSION

Power fluctuations and weak fault ride through capability are the main two issues of the DFIG-based WECS. This paper is aimed at overcoming these two issues by adopting a new topology for the back-to-back converters that interfacing the rotor of the DFIG to the grid by integrating a high temperature superconductor within the DC link. Fractional order proportional integral controller is employed to regulate the energy exchange between the coil and the DC link through a DC-DC chopper. The optimum minimum size of the superconductor and the parameters of the FOPI controller that can result in maximum WECS performance are calculated using the harmony search optimization technique. For all case studies, performance of the investigated DFIG-based WECS with the proposed FOPI controllers is compared with the performance when conventional PI controllers are employed. Results show that harmony search optimization technique can effectively calculate the optimum controllers' parameters along with the minimum size of the superconductor. The proposed controller is very effective in regulating the DFIG output power during wind gust. Results also show that the proposed controller can effectively enhance the low voltage ride through capability of the DFIG during short circuit faults at the point of common coupling. The performance of the FOPI controller outperforms the conventional PI controller that is commonly used by the current practice. In contrary with the existing techniques in the literatures that call for the connection of external FACTS or require a change in the conventional control system of the DFIG-WECS, the proposed technique is modular and can be implemented for both new and existing installation.

REFERENCES

[1] G. Abad, J. Lopez, M. Rodriguez, L. Marroyo, and G. Iwanski, *Doubly Fed Induction Machine: Modeling and Control for Wind Energy Generation*. Hoboken, NJ, USA: Wiley, 2011.
[2] H. T. Jadhav and R. Roy, "A comprehensive review on the grid integration of doubly fed induction generator," *Int. J. Elect. Power Energy Syst.*, vol. 49, pp. 8–18, Jul. 2013.
[3] G. Rashid and M. H. Ali, "A modified bridge-type fault current limiter for fault ride-through capacity enhancement of fixed speed wind generator," *IEEE Trans. Energy Convers.*, vol. 29, no. 2, pp. 527–534, Jun. 2014.
[4] M. S. Yunus, A. Abu-Siada, and M. A. S. Masoum, "Application of SMES unit to improve DFIG power dispatch and dynamic performance during intermittent misfire and fire-through faults," *IEEE Trans. Appl. Supercond.*, vol. 23, no. 4, Aug. 2013, Art. no. 5701712.
[5] J. Lin, Y. Sun, Y. Song, W. Gao, and P. Soensen, "Wind power fluctuation smoothing controller based on risk assessment of grid frequency deviation in an isolated system," *IEEE Trans. Sustain. Energy*, vol. 4, no. 2, pp. 379–392, Apr. 2013.
[6] I. Ngamroo and T. Karaipoom, "Improving low-voltage ride-through performance and alleviating power fluctuation of DFIG wind turbine in DC microgrid by optimal SMES with fault current limiting function," *IEEE Trans. Appl. Supercond.*, vol. 24, no. 5, Oct. 2014, Art. no. 5700805.
[7] A. M. S. Yunus, M. A. S. Masoum, A. Abu-Siada, "Application of SMES to enhance the dynamic performance of DFIG during voltage sag and swell," *IEEE Trans. Appl. Supercond.*, vol. 22, no. 4, Aug. 2012, Art. no. 5702009.
[8] C. Luo, H. Banakar, B. Shen, and B.-T. Ooi, "Strategies to smooth wind power fluctuations of wind turbine generator," *IEEE Trans. Energy Convers.*, vol. 22, no. 2, pp. 341–349, Jun. 2007.
[9] A. F. Abdou, A. Abu-Siada, and H. R. Pota, "Impact of VSC faults on dynamic performance and low voltage ride through of DFIG," *Int. J. Elect. Power Energy Syst.*, vol. 65, pp. 334–347, Feb. 2014.
[10] A. F. Abdou, H. R. Pota, A. Abu-Siada, and Y. M. Alharbi, "Application of STATCOM-HTS to improve DFIG performance and FRT during IGBT short circuit," in *Proc. Australas. Univ. Power Eng. Conf. (AUPEC)*, Sep./Oct. 2014, pp. 1–5.
[11] A. M. S. Yunus, A. Abu-Siada, and M. A. S. Masoum, "Improving dynamic performance of wind energy conversion systems using fuzzy-based hysteresis current-controlled superconducting magnetic energy storage," *IET Power Electron.*, vol. 5, no. 8, pp. 1305–1314, Sep. 2012.
[12] M. Benbouzid, S. Muyeen, and F. Khoucha, "An up-to-date review of low-voltage ride through techniques for doubly-fed induction generator-based wind turbines," *Int. J. Energy Convers.*, vol. 3, no. 1, pp. 1–9, 2015.
[13] W. Guo, L. Xiao, and S. Dai, "Fault current limiter-battery energy storage system for the doubly-fed induction generator: Analysis and experimental verification," *IET Gener. Transmiss. Distrib.*, vol. 10, no. 3, pp. 653–660, Feb. 2016.
[14] M. I. Mosaad, "Control of self excited induction generator using ANN based SVC," *Int. J. Comput. Appl.*, vol. 23, no. 5, pp. 22–25, Jun. 2011.
[15] M. I. Mosaad and F. Salem, "Adaptive voltage regulation of self excited induction generator using FACTS controllers," *Int. J. Ind. Electron. Drives- Inderesci. Publishers*, vol. 1, no. 4, pp. 219–226, 2014.
[16] M. I. Mosaad, "Model reference adaptive control of STATCOM for grid integration of wind energy systems," *IET Electr. Power Appl. J.*, vol. 12, no. 5, pp. 605–613, May 2018.
[17] C. Wessels, F. Gebhardt, and F. W. Fuchs, "Fault ride-through of a DFIG wind turbine using a dynamic voltage restorer during symmetrical and asymmetrical grid faults," *IEEE Trans. Power Electron.*, vol. 26, no. 3, pp. 807–815, Mar. 2011.

[18] Y. M. Khamaira, A. Abu-Siada, S. Islam, and M. S. Masoum, "A new topology for doubly fed induction generator to improve the overall performance of wind energy conversion system," *Elixir Elect. Eng. J.*, vol. 73, pp. 26432–26435, Aug. 2014.

[19] M. Y. Khamaira, A. Abu-Siada, and S. Islam, "Application of high temperature superconductor to improve the dynamic performance of WECS," presented at the IEEE PES Gen. Meeting, Denver, Colorado, USA, Jul. 2015.

[20] W. Guo, L. Xiao, and S. Dai, "Enhancing low-voltage ride-through capability and smoothing output power of DFIG with a superconducting fault-current limiter–magnetic energy storage system," *IEEE Trans. Energy Convers.*, vol. 27, no. 2, pp. 277–295, Jun. 2012.

[21] T. Karaipoom and I. Ngamroo, "Optimal superconducting coil integrated into DFIG wind turbine for fault ride through capability enhancement and output power fluctuation suppression," *IEEE Trans. Sustain. Energy* , vol. 6, no. 1, Jan. 2015, Art. no. 2355423.

[22] I. Ngamroo, "Optimization of SMES-FCL for augmenting FRT performance and smoothing output power of grid-connected DFIG wind turbine," *IEEE Trans. Appl. Supercond.*, vol. 26, no. 7, Oct. 2016, Art. no. 3800405.

[23] M. I. Mosaad and H. S. Ramadan, "Power quality enhancement of grid-connected fuel cell using evolutionary computing techniques," *Int. J. Hydrogen*, vol. 43, no. 25, pp. 11568–11582, Jun. 2018.

[24] J. Zhong and L. Li, "Tuning fractional-order $PI^{\lambda}D^{\mu}$ controllers for a solid-core magnetic bearing system," *IEEE Trans. Control Syst. Technol.*, vol. 23, no. 4, pp. 1648–1656, Jul. 2015.

[25] A. Dabiri, B. P. Moghaddam, and J. A. T. Machado, "Optimal variable-order fractional PID controllers for dynamical systems," *J. Comput. Appl. Math.*, vol. 339, pp. 40–48, Sep. 2018.

[26] D. Pullaguram, S. Mishra, N. Senroy, and M. Mukherjee, "Design and tuning of robust fractional order controller for autonomous microgrid VSC system," *IEEE Trans. Ind. Appl.*, vol. 54, no. 1, pp. 91–101, Jan./Feb. 2018.

[27] A. Petersson, *Analysis, Modeling and Control of Doubly-Fed Induction Generators for Wind Turbines*. Gothenburg, Sweden: Chalmers Univ. Technol., 2005.

[28] S. Li and T. A. Haskew, "Analysis of decoupled d-q vector control in DFIG back-to-back PWM converter," in *Proc. IEEE Power Eng. Soc. Gen. Meeting*, Jun. 2007, pp. 1–7.

[29] R. Pena, J. C. Clare, and G. M. Asher, "Doubly fed induction generator using back-to-back PWM converters and its application to variable-speed wind-energy generation," *IEE Proc.- Electr. Power Appl.*, vol. 143, pp. 231–241, May 1996.

[30] A. F. Abdou, A. Abu-Siada, and H. R. Pota, "DFIG fault ride through improvement during VSC faults," *Can. Res. Develop. Center Sci. Cultures*, vol. 5, no. 1, pp. 13849–13854, Feb. 2013.

[31] J. Viola, L. Angel, and J. M. Sebastian, "Design and robust performance evaluation of a fractional order PID controller applied to a DC motor," *IEEE/CAA J. Automatica Sinica*, vol. 4, no. 2, pp. 304–314, Apr. 2017.

[32] M. I. Mosaad, N. I. Elkalashy, and M. G. Ashmawy, "Integrating adaptive control of renewable distributed switched reluctance generation and feeder protection coordination," *Electr. Power Syst. Res.*, vol. 154, pp. 452–462, Jan. 2018.

[33] *Voltage Characteristics of Electricity Supplied by Public Distribution Systems*, Standard EN 50160, 1999.

[34] D. Manjarresa, I. Landa-Torres, S. Gil-Lopez, J. D. Ser, M. N. Bilbao, S. Salcedo-Sanz, and Z. W. Geem, "A survey on applications of the harmony search algorithm," *Eng. Appl. Artif. Intell.*, vol. 26, no. 8, pp. 1818–1831, Sep. 2013.

[35] A. Verma, B. K. Panigrahi, and P. R. Bijwe, "Harmony search algorithm for transmission network expansion planning," *IET Gener., Transmiss. Distrib.*, vol. 4, no. 6, pp. 663–673, Jun. 2010.

[36] Z. W. Geem, J. H. Kim, and G. V. Loganathan, "A new heuristic optimization algorithm: Harmony search," *Simulation*, vol. 76, no. 2, pp. 60–68, 2001.